ETH

Eidgenössische Technische Hochschule Zürich
Swiss Federal Institute of Technology Zurich

Improved measurement method for spatial-dependent photo response

Semester Thesis

Samuel Gyger

February 28th, 2016

Supervisor: Dr. Anton Potočnik

Group leader: Prof. Andreas Wallraff

Group: Quantum Device Lab, ETH Zürich

Abstract

The change in the RF-reflection coefficient, induced by impinging laser light on a superconducting resonator, is called photo response. The thesis investigates spatial dependence of this change in a niobium based lumped element resonator using a fast new measurement method. The method was then used to investigate the change due to different temperatures between 3.05 K and 4.5 K. Modulation of the laser intensity is used for a time dependent investigation of the photo response.

Additionally the thesis contains information on the move of the setup to a new room.

i

Contents

Chapter 1

Introduction

Superconducting circuits with two-level systems are a common tool used today in the field of quantum computation and digital as well as analog quantum simulation [1]. A necessary process is to tune the parameters inside the system, which is often done by flux lines or global magnetic fields [2, 3]. Superconducting circuits, called kinetic inductance detectors, are used to detect single X-ray photons or low intensity light in the mm-range [4, 5]. This thesis explores a so-called laser scanning microscope (LSM) which combines both techniques.

Impinging light on a superconductor breaks cooper pairs into quasi particles [6] and thereby increased the local resistivity of the system as well as the kinetic inductance. Several methods to investigate the properties of superconductors were developed and summarized as laser scanning microscopy (LSM) for superconductors [7]. A method based on the change in transmitted power, the photoresponse, at high frequencies was used to investigate the spatial current density distribution in high temperature superconductors [8]. The squared dependence on current density as well as a sublinear response on RF power on the spatial photoresponse was investigated [9]. This work inspired a recent master thesis investigating LSM in superconducting lumped element resonators at liquid helium temperatures [10]. It introduces a theory explaining the measured effects as well as several measurement methods.

LSM can be used to search for manufacturing defects through identifying unknown modes by analyzing the spatial current distribution. The laser could also be used as a non-interfering tuning method for a superconducting resonator. This would open another dimension for controlling a quantum system by reducing the amount of control lines between the room temperature electronics and the mK superconducting chip.

This semester-thesis uses a niobium based superconducting lumped element

circuit to further investigate the influence of LSM. It introduces a faster measurement method to identify the photoresponse in lumped element circuits. This method is used to investigate the spatial dependence of the photoresponse as well as the temperature dependence for the range between 3 K to 4.5 K In the end the temporal dynamics of the photoresponse are investigated. Chapter 2 offers a brief summary on the relocation of the setup in a new room as well as introducing its components. Chapter 3 briefly introduces the photoresponse and the available measurement methods. Chapter 4 presents the results and a summary of the work can be found in chapter 5.

Chapter 2

Setup

This section discusses the setup used in the experiments. It consist of an attoCube system used for positioning the laser, an optical setup and a microwave setup. The move of the setup into a new room is also discussed.

The setup contains a fridge using a cryocooler providing a minimum temperature of 3.02 K and providing a vacuum on the order of 10^{-7} mBar. The photo response measurement is based on measuring the change in the RF behavior influenced by an optical input. It needs an optical setup and the possibility to acquire microwave signals.

2.1 Microwave Setup

Figure 2.1 shows the microwave setup used in the experiments. The microwave signal is generated by a signal generator SMB100A and then fed into the fridge where a directional coupler splits incoming and returning signal in two different lines. The signal reflected from the studied chip is amplified first at 4 K and later at room temperature. The amplified signal is down converted to 0 Hz or and intermediate frequency (IF) and then measured by the ASC500, a scanning probe microscopy (SPM) controller or the FPGA, an in-house build measurement platform. The red box denotes the down-conversion arm that exists twice where the red symbols are the alternative connections for the second arm.

The second arm provides a phase reference to preserve the phase relation between the local oscillator (LO) and the RF input. It is not preserved during a frequency change at the signal generators. The signal from the RF generator is fed through a -20 dB attenuator, before being amplified in a down conversion arm similiar to the one amplifying the reflection signal from the fridge. The signal is fed into input B at the FPGA. A constant phase relation is achieved by multiplying input A with complex conjugated input B.
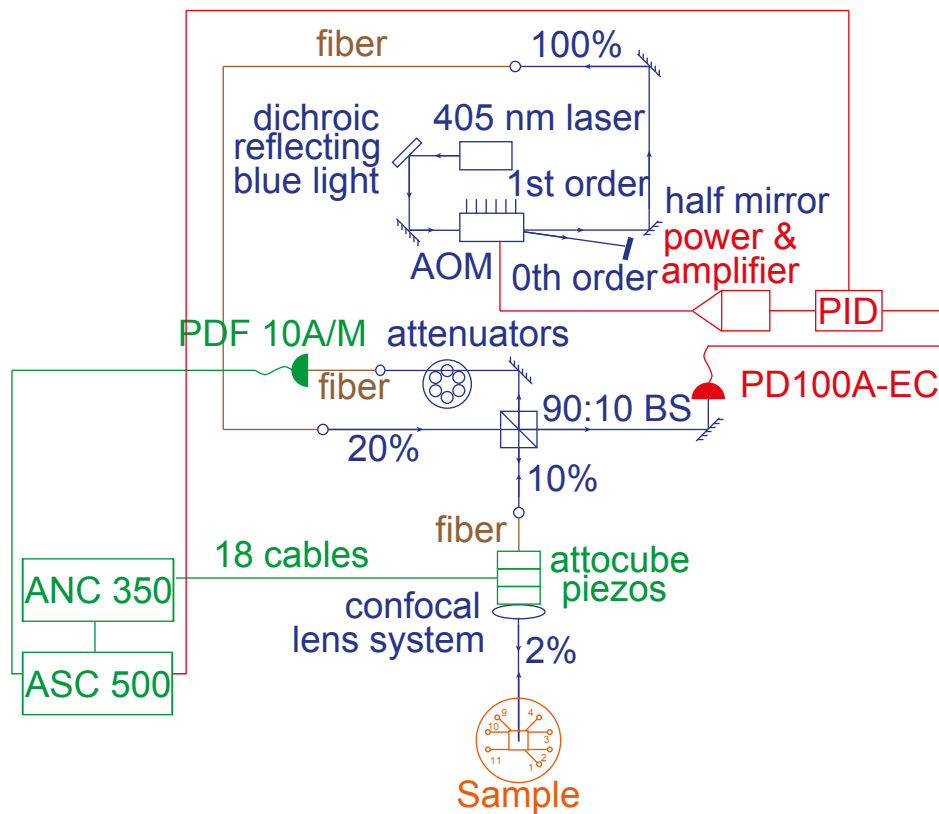
Figure 2.1: The microwave setup used in the experiments. The red dashed box exists twice. The second time as a reference arm, where it is connected with the red lines. Based on [10].

Figure 2.2: The optical setup used in the experiments. Based on [10].

2.2 Optical Setup

The laser is used to stimulate the photo response and observe the chip through reflected laser light.

Figure 2.2 shows the optical setup used in the experiments. A laser at 405 nm wavelength is modulated using an acousto-optic modulator (AOM). The AOM diffracts part of the laser beam. The intensity of the diffracted beam is controlled by the amplitude of the input to the AOM. It is afterwards fed to a 90:10 beamsplitter and the transmitted beam is measured using a PIN-photodiode PDA100A-EC. A feedback loop, using a PID controller, stabilizes the output power of the diffracted beam by changing the AOM input. A modulation signal can be fed as a set-point to the PID controller to modulate the laser intensity. The reflected beam is coupled into a fiber leading into the fridge. A confocal microscope rig is mounted on an attoCube positioning setup above the sample. The reflected light is collected by the microscope and attenuated before being measured using a femtowatt Si-photodiode PDF10A/M.

2.2.1 Positioners

The confocal microscope inside the fridge can be moved in three dimensions with two different accuracies and ranges. The piezo stepper system ANPx101 has a range of 5 mm with an accuracy of 1 um in our setup. A piezo scanner ANSxyz100 with a range of 30 μm x 30 μm x 15 μm at 4 K allows a nanometer resolution. An ANC350 motion controller is used to control the piezo scanners.

Figure 2.3 shows the working principle of the stepper system [11]. A movable table rests loosely on a guiding rod mounted to a piezo crystal. The expanding crystal, due to increase of the voltage V_{Drive}, moves the table through friction. If the position of the guiding rod changes quickly, the heavier table rests at its original position, allowing the piezo crystal to contract and move it a little further by expanding slowly again. A saw-tooth control voltage leads to a forward or backward motion of the table. The voltage drop measured at the guiding rod allows to determine the position of the table.
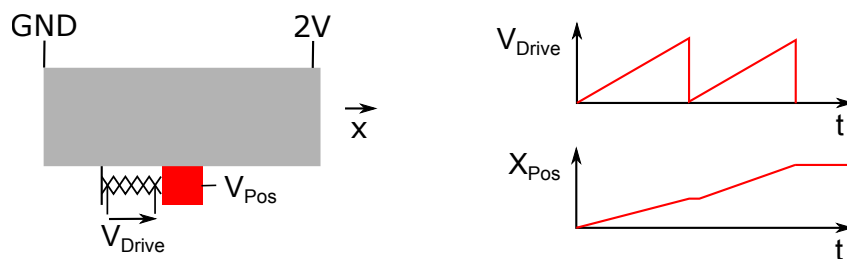

Figure 2.3: The principle of the stepper is based on the inertia of the gray table, that does not move on a fast contraction of the piezo. The red box is the guiding rod. The drawn spring is the piezo crystal.

The stepper systems allows to observe larger areas of the chip. Three parameters, amplitude, frequency and amplitude control are available to optimize the accuracy. The amplitude changes the step size on each expansion of the piezo crystal and the frequency influences the speed of the table. The amplitude control mode sets the parameter the controller tries to keep constant, while changing the other two. Possible choices are the amplitude, the speed or the step width.

The ANC350 is controlled by the ASC500, a scanning probe microscopy (SPM) controller. It allows to conduct position dependent measurements e.g. the photoresponse of the whole sample, that is recorded using the attoCube steppers. The control values for the piezos need to be optimized to achieve a good stepping accuracy. The step scanning feature prepares the confocal microscope at a chosen position. It approaches the first mea-
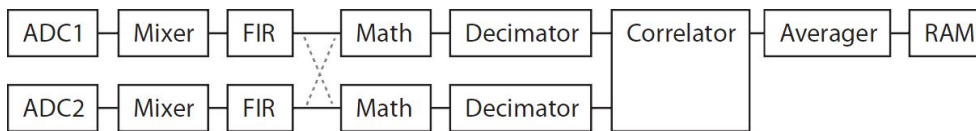
Figure 2.4: The signal processing pipeline implemented in the FPGA. [13]

surement position with an accuracy defined by the Appr(oach) Range value. Once the measurement is started it will go forward to the first position to measure.

The current position of the stepper is available as an analog input, that is averaged during the settling average time. Once the position is equal or bigger than the target position, the system records a data point. Afterwards it increases the target position. If the step of the stepper is larger then the required position, several points are measured at the same position until the target position becomes larger then the current position.

The settings in ANC350 and ASC500 have to be optimized. The procedure and the settings used in this experiment are described in table A.4. The data sheets lists a minimal step size of 10 nm and a sensor position resolution of $\approx$ 200 nm. This suggests that better performance should be possible [12]. Sources for this low resolution is the noisy measurement signal of the position, that is due to non-existing shielding of the cable, and the high necessary voltage for the $\hat{y}$ position to move, were a contact with the company suggests a replacement of the positioner device.

2.3 Data Acquisition

The setup allows two different ways to acquire data. The first is the SPM Controller ASC500, the other a Virtex 6 based, in-house build, FPGA measurement platform. The SPM controller contains an build-in lock-in amplifier and allows the measurement of the photoresponse based on the change in amplitude due to a modulated laser signal.

2.3.1 FPGA measurement platform

The FPGA measurement platform is build on a Virtex6 based digtial signal processor (DSP) board. The correlator application, used in this experiment, allows to measure correlation functions of microwave signals. Figure 2.4 shows the implemented signal processing pipeline, that contains an analog-digital converter, a digital mixer, mathematical functions, filters, decimator and the correlator. At the end of the pipeline several consecutive measurements can be averaged.

The digital mixer in the FPGA is working at an intermediate frequency (IF) of 250 MHz. It allows the observation of phase and amplitude using only one quadrature of the analog IQ mixer in the microwave setup shown in section 2.1.

The pipeline from the AD converter up to the decimator is continuously processing data with a sample time of 1 ns. At the decimator samples can be dropped and at an incoming trigger event, 8192 samples are collected to a measurement block and fourier transformed using FFT. The block continues to the correlator. The correlation feature, that is not used in this experiments, can be turned off by enabling the averaging mode. Additionally the differential mode (Diff Mode) allows to subtract subsequent measurements. Between 1 and 2^{31} measurements blocks can be averaged before the measurement result is transferred to CleanSweep, a LabView program. On the computer an inverse DFT is applied and a measurement trace of 8.192 μs is available.

CleanSweep allows to run automatized measurements varying multiple parameters as e.g. power and frequency.

2.3.2 SPM controller ASC500

The SPM controller ASC500 contains a build-in AD converter, DA converter and a lock-in amplifier. It allows to create output signals controlling the ASC350 position controller to make spatial-dependent measurements. Two different acquisition modes were used in this experiment.

The scanning mode uses the piezo scanners to record small areas of 30 um x 30 um. At every point on a measurement grid the input is averaged over a given time e.g. 5 ms. Without a feedback from the piezo scanners only an open-loop measurement is possible.

The second method is a closed-loop measurement using the step scanners and controls the position through the ANC350 as explained in section 2.2.1. The data from the AD converter or the signal fed through the lock-in amplifier can be recorded at each point on the measurement grid.

2.4 Move of the setup

Samuel Gyger moved the setup from B22 to the new room B25 on Novemeber 2nd, 2015. The optical part was moved to a breadboard, mounted on an optical table. All the devices were disconnected, reordered and reconnected at the new location. Several broken connections to the temperature sensors were fixed. Wiring diagrams for the temperature sensors and the attoCube piezos were created in appendix A.5.

Two measurements verified the correct operation of the setup.

Table 2.1: *Photo response measurements using ASC500. The sample is illumi-nated with a 5 kHz modulated laser light. The RF-reflection measurement is down-converted to DC, amplified using a lock-in amplifier. The photo response is spatially recorded with a resolution of* 1 μm.

| December 2014 | January 2016 |
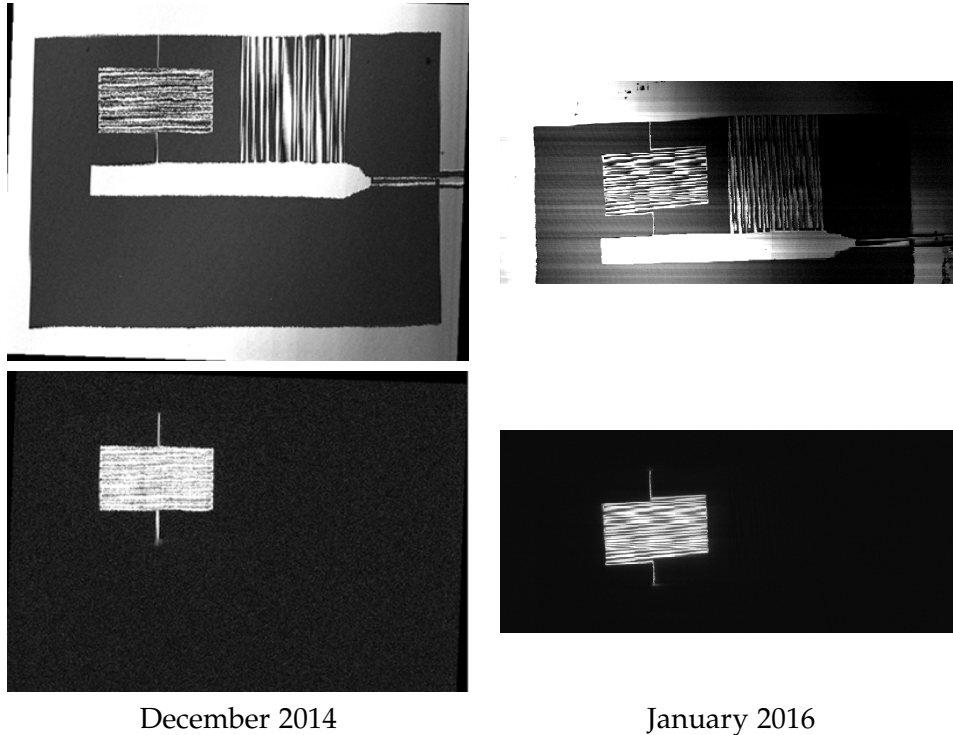
2.4.1 Cooldown

The cool-down process on December 3rd, 2015 was compared with data from July 10th, 2015 in appendix A.2. The cooling time from 300 K to 4 K was ≈ 6 hours in both instances and shows similar features. The same final temperature was reached and one can conclude that the cooling process still works.

2.4.2 Stepscanner image of reflection

Using the step-scanner feature of the control software of the ASC500, Daisy version 2.6, a 800 μm x 350 μm area was measured with a 1 μm x 1 μm resolution. The recorded image is shown in Table 2.1. The comparison image was measured by Anton Potočnik in December 2014.

The blurred lines in the center of the image are due to the steps in $\hat{y}$ direction being sometimes to large, this leads to the same line being measured multiple times. A similar error is seen at the capacitor. The change in inten-

sity is due to the sample being tilted in relation to the microscope, as seen in appendix A.3, so it is further away than the focal length.

Measurements using different positions of the laser show similar visually observed accuracies. The fluctuations in each line of the picture show that the stability of the laser intensity decreased. One explanation could be coupling of other signals to the control cables of the ASC500, leading to small changes in the axis used for focusing.

Chapter 3

Explaining the photo response

This chapter explains the origin of the photo response and presents three different ways to measure it.

3.1 The resonator

The photo response is measured with a superconducting circuit containing a resonator. In case of the typical phase change length of the electromagnetic waves being much larger than the circuit it can be simplified in a lumped element model as seen in fig. 3.1. [14]

Using the constitutive relations

$$i(t) = C\frac{du(t)}{dt} \tag{3.1}$$

for the capacitor and
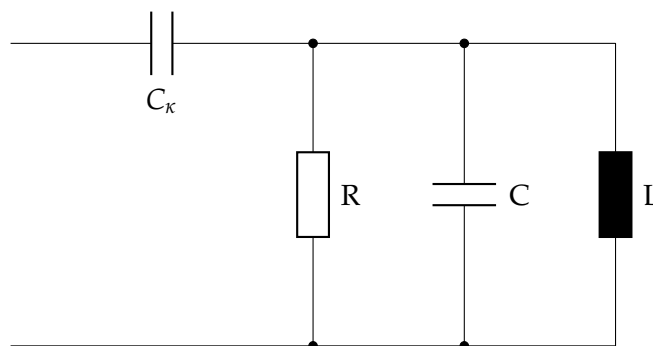
$$u(t) = L\frac{di(t)}{dt} \tag{3.2}$$

Figure 3.1: The harmonic oscillator

for the inductor, were C is the capacitance, L is the inductance, $i(t)$ is the current flowing through the element and $u(t)$ is the voltage across the element, one can derive the impedance of the circuit depending on the frequency to be

$$Z(\nu) = \frac{1}{i2\pi\nu C_\kappa} + \left(R + i2\pi\nu L + \frac{1}{i2\pi\nu C} \right)^{-1} \qquad (3.3)$$

where i is the imaginary unit, R is the internal resistance, L is the internal inductance, C is the internal capacitance and C_κ is the coupling capacitance.

Assuming a week coupling, the resonance frequency is then given [15] by

$$\nu_0 = \frac{1}{2\pi\sqrt{LC}}. \qquad (3.4)$$

The reflection coefficient of such a system can be approximated by a Lorentzian shaped resonance curve [16].

$$\Gamma(\nu) = \frac{\kappa}{\frac{\gamma+\kappa}{2} + i2\pi(\nu - \nu_0)} - 1 \qquad (3.5)$$

were Γ is the reflection coefficient, κ is the external loss rate and γ is the internal loss-rate. ν_0 is the resonance frequency and ν is the frequency, the reflection coefficient is evaluated at.

In the experiments of this thesis the sample M36 LM1 1 is used. The measurements are done on the resonator displayed in fig. 3.2 connected to port 9. It has 25 fingers at the capacitor, 27 windings in the inductor and a coupling capacitor with 2 fingers. The layout mask can be found in the appendix A.4.

If not mentioned differently, the laser light was focused on the line in the center of the inductor.

3.2 The photo response

The superconductor contains two types of charge carriers: the Cooper pairs, that provide the interesting lossless direct current, and the quasi-particles, exhibiting electron-like behavior. The idea of this two different particles was early on captured in the Gorter-Casimir two-fluid model using two channels, one being lossless, the other lossy [17].

The lossy channel shows resistive behavior, while the lossless channel shows inductive behavior due to the kinetic inductance. While self-inductance is dependent on the geometric features and stores energy in the magnetic field, kinetic inductance is dependent on energy stored in the movement of the
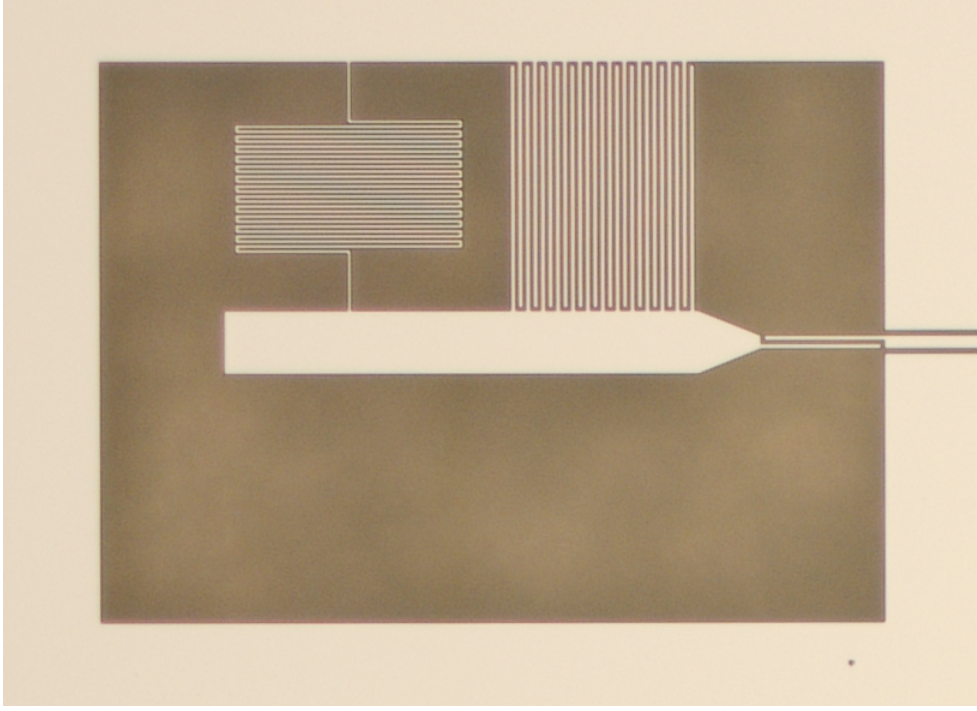
Figure 3.2: The resonator used for all the experiments with 27 inductor windings, 25 fingers at the capacitor and the coupling is realized with a 2 finger capacitor.

charge carriers. For electrons this only becomes relevant at optical frequencies, but due to the slow relaxation rate of Cooper pairs, it is a relevant contribution to the inductance at MW frequencies [10].

Illuminating the superconductor with a laser, that has much higher energy e.g. 3.06 eV at 405 nm than the energy gap e.g. 2.91 meV [18] in niobium, breaks up many Cooper pairs into quasi particles.

This process leads to a change of the resonance frequency eq. (3.4) due to an decrease in the kinetic inductance and an increase of the internal loss-rate due to the created lossy charge carriers. The result is a shifted and broader Lorentzian curve,

$$\Gamma_{\text{LaserOn}}(\nu) = \frac{\kappa}{\frac{\gamma + \delta\gamma + \kappa}{2} + i2\pi(\nu - \nu_0 - \delta\nu)} - 1, \tag{3.6}$$

were $\delta\gamma$ is the increase in the internal loss-rate and $\delta\nu_0$ is the shift in the resonance frequency.

The photo response, investigated in this semester thesis, is the difference between the shifted Lorentzian curve eq. (3.6) and the original one eq. (3.5),

$$PR = \Gamma_{\text{LaserOn}} - \Gamma, \tag{3.7}$$

13

.

Chen [10] shows that this interaction between the laser and the superconductor is depended on the local density of Cooper pairs and that the change in the amplitude of the photo response is proportional to J^2, were J is the current density. Several researchers have used this effect to probe the current density in superconducting resonant systems [8, 7].

3.3 Measuring the photo response

There are several ways of measuring the photo response introduced in the last section.

3.3.1 Static photo response measurement

The static photo response is measured by acquiring the reflection coefficient twice at all frequencies, first with the laser turned on and then with the laser turned off. This allows to reconstruct all relevant parameters by fitting eq. (3.5). Disadvantage of this method is the long measurement time.

3.3.2 Interleaved photo response measurement

Subsequent measurements with laser turned on and laser turned off are taken by aligning the trigger of the FPGA with the modulation of the laser intensity. The differential mode, implemented in the FPGA, subtracts every other measurement taken by the FPGA and returns the photo response as a result [16]. Advantages are the single measurement run that needs to be done and less influence of laser heating as claimed by Chen [16]. Disadvantages are a noisy phase measurement in the regions with low amplitude, a lot of fitting parameters and a whole frequency sweep for every changed laser parameter.

3.3.3 Single point photo response measurement

All the presented measurement methods have the disadvantage that they need a lot of time to measure because every frequency has to be swept once or twice, while only two parameters $\delta\nu_0$ and $\delta\gamma$ are of interest. This new measurement method allows to compute this two parameters from a single measurement.

Subtracting the inverse of the reflection coefficient with and without laser leads to

$$\frac{1}{\Gamma_{\text{LaserOn}} + 1} - \frac{1}{\Gamma + 1} = \frac{1}{\kappa}\left(\frac{\delta\gamma}{2} - i2\pi\delta\nu_0\right) \tag{3.8}$$

14

were κ has to be previously determined e.g. by fitting to a reflection measurement at multiple frequencies with the laser turned off.

The two parameters can then be reconstructed from a measurement at a single frequency. This result is theoretically independent of the measurement frequency. In practice it is strongly dependent on the phase noise as seen in the following equation.

$$
\begin{aligned}
&\frac{1}{|\Gamma_{\mathrm{lo}} + 1| \exp i\phi_{\mathrm{lo}} + ie} - \frac{1}{|\Gamma + 1| \exp i\phi + ie'} \\
&= \exp -i(\phi_{\mathrm{lo}} + e) \left(\frac{1}{|\Gamma_{\mathrm{lo}} + 1|} - \frac{1}{|\Gamma + 1|} \exp -i(\phi - \phi_{\mathrm{lo}} + e - e') \right)
\end{aligned}
\tag{3.9}
$$

where Γ_{lo} is the reflection coefficient with laser on, and Γ with laser off. ϕ is the argument of the complex number $\Gamma + 1$. e and e' are uncorrelated random error terms.

Equation (3.9) shows that the error will become significant once the difference in the phase of the two measurements is small. For an accurate measurement result it is necessary to choose a frequency for measurement were the difference in phase is as large as possible. This is close to the resonances of either the laser on or the Laser off system. The measurement then allows the same accuracy as the static photo response measurement or the interleaved mode measurement without the necessity to fit the values and a much faster measurement time.

Chapter 4

Measurements of the photo response

This chapter first compares the measurement methods introduced in the previous chapter. Afterwards it presents a spatial dependent measurement of the photo response, measurements of the temperature dependence between 3 K and 4.5 K and closes with the temporal analysis of the photo response.

4.1 Comparison of measurement methods

4.1.1 Comparing static photo response measurement and interleaved measurement

The three measurement methods introduced in Section 3.3 were compared in this measurement. Four measurements at 3.3 K with -97 dBm RF-power at the sample were conducted. A focused laser at 11.7 µW pointed at the center of the inductor. The first measurement had the laser stabilized by the PID controller. The second measurement was conducted with a rectangular modulated laser beam at 5 kHz. The third measurement had no diffraction beam at the AOM, by setting the set-point off the PID Controller to 0 V. For the last measurement the laser was completely turned off.

The phase and the photo response can be seen in fig. 4.1 to be equal up to a scaling factor. Part of this scaling factor is due to the signal processing chain in the FPGA. In the static measurement N block with laser on and N items with laser off are recorded and averaged. These two averages are subtracted to get the photo response.

$$PR_{\text{static PR}} = \frac{1}{N}\sum_N \Gamma_{\text{Laser on}} - \frac{1}{N}\sum_N \Gamma_{\text{Laser off}} \qquad (4.1)$$

In the interleaved mode half of the N samples acquired are with a laser turned on, the other half are with a laser off and subtracted before taking
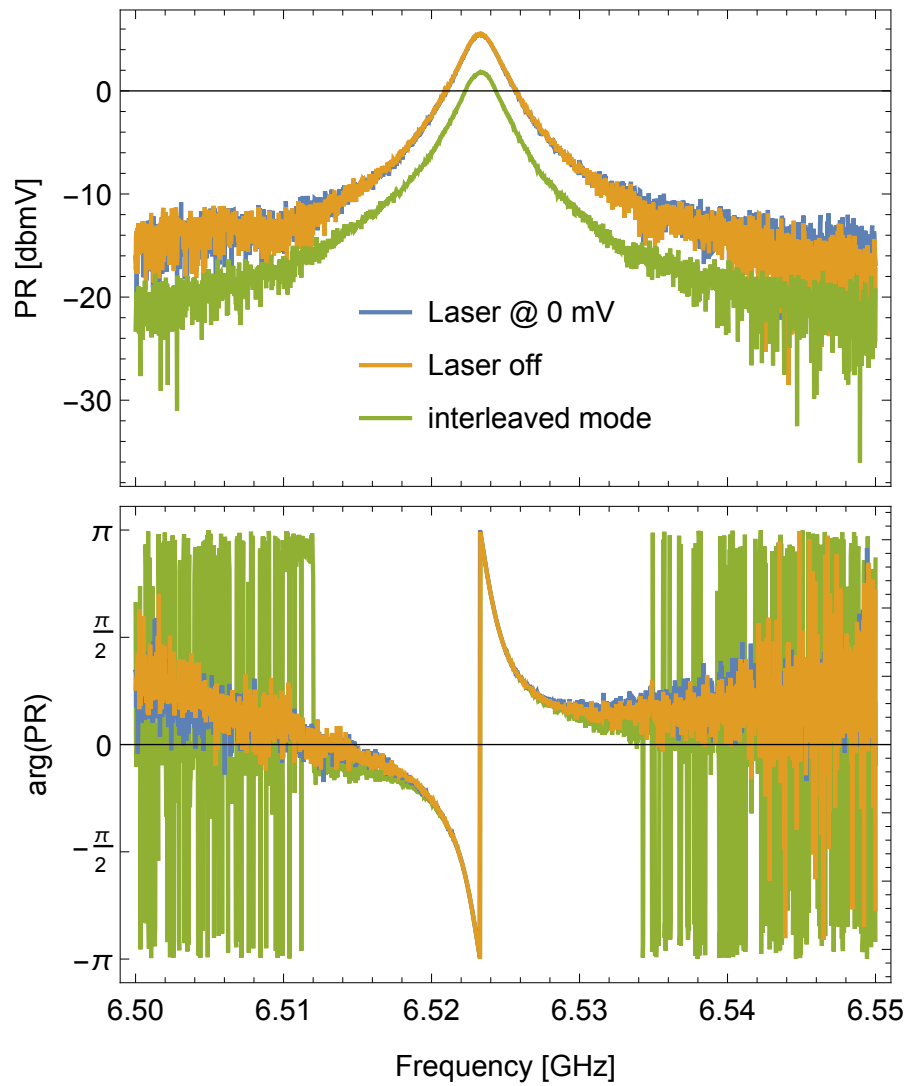
Figure 4.1: The different measurement methods show the same phase behavior and a scaled amplitude. T = 3.3 K, −97 dBm RF power, 11.7 µW laser power focused at the center of the inductor.
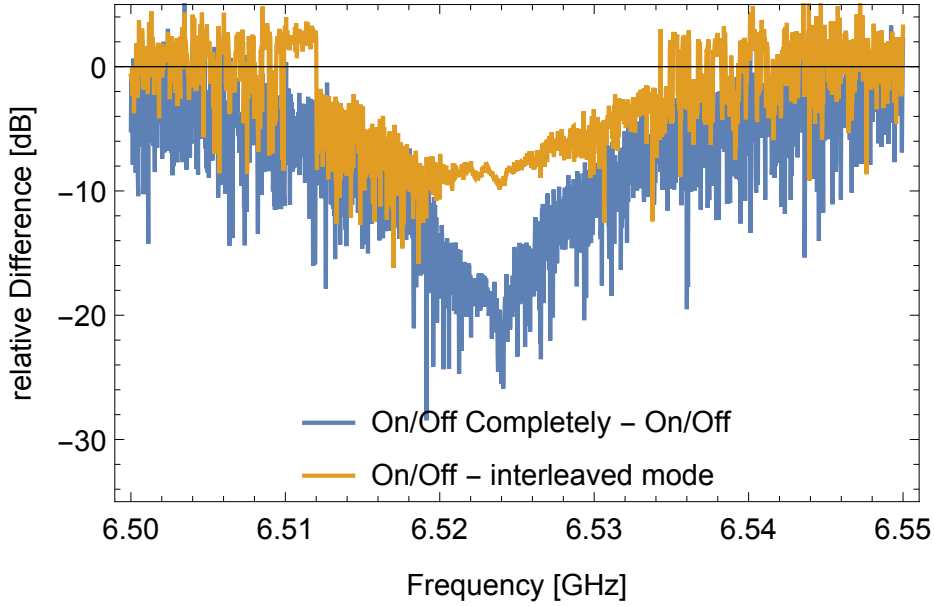
Figure 4.2: The error of the different measurement methods compared to the Laser at the set-point 0 mV. The interleaved mode was corrected for the FPGA scaling difference of 2.

the mean.

$$PR_{\text{interleaved}} = \frac{1}{N} \left(\sum_{N/2} \Gamma_{\text{Laser on}} - \sum_{N/2} \Gamma_{\text{Laser off}} \right) \tag{4.2}$$

With half the samples in the second mean, this leads to a factor of two between the two measurements.

Figure 4.2 shows the relative difference between the static measurement and the interleaved mode, after correcting for the factor of two, is -8 dB. The relative difference between the laser turned of using the AOM and the laser completely turned off using the laser power supply is less then -20 dB in the frequency range around the resonance.

Both measurements were fitted using eq. (3.7), where the external loss rate $\kappa = 2.01$ MHz and the internal loss rate $\gamma = 702$ kHz where taken from a fit of eq. (3.5) to the measurement with the laser set to the set-point of 0 mV. The fitted values are shown in table 4.1 and show a difference in $\delta\omega0$ of 7.5% and in $\delta\gamma$ of 21%.

4.1.2 Comparing single-point measurement

The single-point measurement method in Section 3.3.3 allows a faster measurement of the photo response to get $\delta\gamma$ and $\delta\nu_0$. In theory the measure-

Table 4.1: Fitted values for the three measurement methods.

	$\Delta\gamma$ [kHz]	Δf_0 [kHz]
Laser @ (On, 0 mV)	26.21	-435.2
Laser @ (On, Off)	24.48	-435.1
Differential Mode	33.28	-404.8

ment frequency for this single point is arbitrary, due to noise this is not true in practice.

A measurement at 3.3 K with -97 dBm RF-power and a focused laser at 11.7 µW pointing at the center of the inductor was conducted for several frequencies, similar to the static photo response measurement. A second measurement without laser was used to estimate $\kappa = 2.166$ MHz. Comparing the calculated photo response, using the $\delta\nu_0$ and $\delta\gamma$, with a static photo response measurement, a relative difference of less then -10 dB was observed at the resonance frequencies. Away from them the noise in the phase makes the reconstruction impossible.

Measuring the photo response at the frequency of the resonance allows an accurate calculation of $\delta\nu_0$ and $\delta\gamma$.

4.2 Measuring the spatial distribution of the photoresponse

With the single-point measurement method introduced in Section 3.3.3 it is possible to do fast measurements with changed laser parameters i.e. the position of the laser. The measurements were conducted at 3.3 K with RF-powers between -91 dBm and -121 dBm and laser power of 11.7 µW focused at the sample. Section 4.2 shows the positions of the measurement that was conducted along the cross-section of a line in the center of the inductor.

The reflection measurement with the laser at a setpoint of 0 mV was done in 25 kHz steps to get a fitted κ ranging between 2.162 MHz and 2.167 MHz. For the single point measurements with the laser, 2 million FPGA measurements were averaged, to compensate for fluctuations seen in the laser intensity.

The measurements at different positions seen in fig. 4.5 show an increased shift of ν_0 and γ suggest an increased current density at the edge of the inductor line. The increased current density at the edge of thin strip lines is a solution to Maxwell's equation in thin conducting strips [19, Chapter 3.12] independent of its superconducting properties.
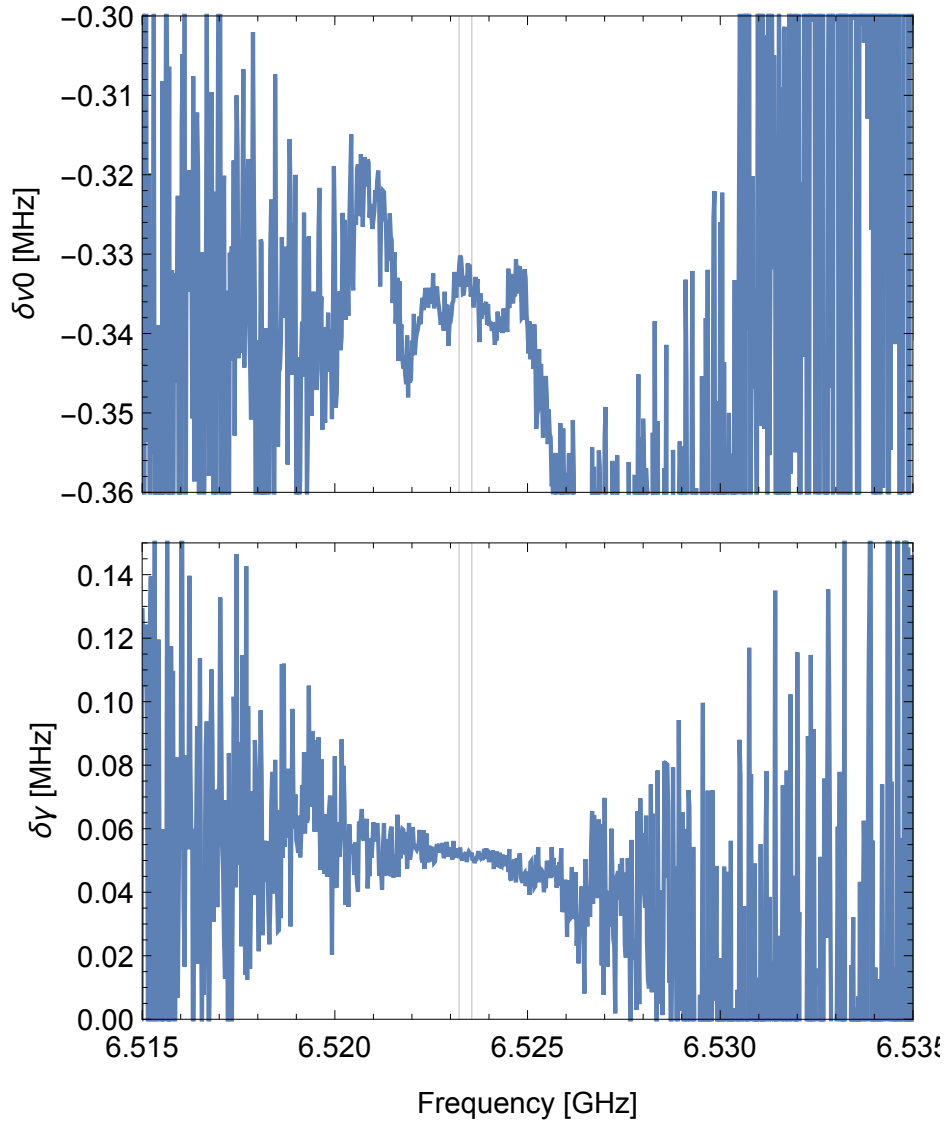
Figure 4.3: The estimates of δv_0 and $\delta \gamma$ based on the single-point measurement at different frequencies. The left gray line shows the resonance frequency with the laser on at 11.7 µW, the right gray line without the laser at set-point 0 mV. $T = 3.3$ K and -97 dBm RF-power
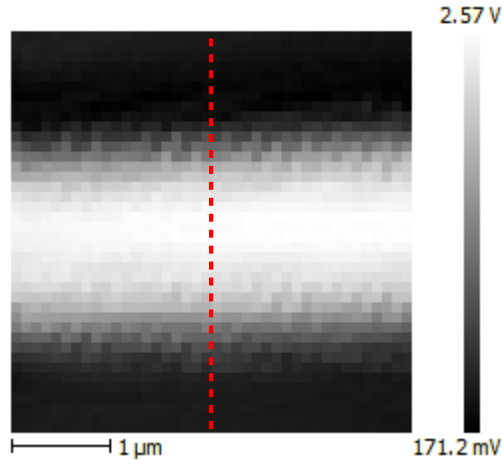
Figure 4.4: Inductor line in the center of the inductor. Dashed red line shows the cut line were the photo response was measured. The laser power was 11.7 μW *at* $T = 3.3\ K$

8 out of 11 measured powers show this increase of current density at the edges, as investigated by [9, 8]. The ratio between peak and valley was 1.30 for -91 dBm and 1.24 for -121 dBm at the sample.

For the 3 powers, shown in fig. 4.6, only one peak that is shifted to the side can be observed. This is due to uncertainties in our measurements such as laser intensity or focus shifts. The roughness of our measurements can be explained by a large angle between the microscope and the chip explained in appendix A.3 as well as other noise sources due to positioning.

This example shows that a fast measurement can be implemented using the scheme described in section 3.3.3. An implementation in Clean Sweep would allow a 2-dimensional scan of the photo-response.

The same measurement is used to look at the relationship between RF power and the photo response in fig. 4.7. Chen [16] states and experimentally verifies the relationship of $PR \propto \sqrt{Pwr_{\mathrm{mw}}}$ were PR is the photo response and Pwr_{mw} the RF power. An exponential fit of the photo response at the center of the inductor line leads to an exponent of 0.48 with a confidence interval of 0.40 to 0.55 given by the fitting function assuming a Gaussian independent error.
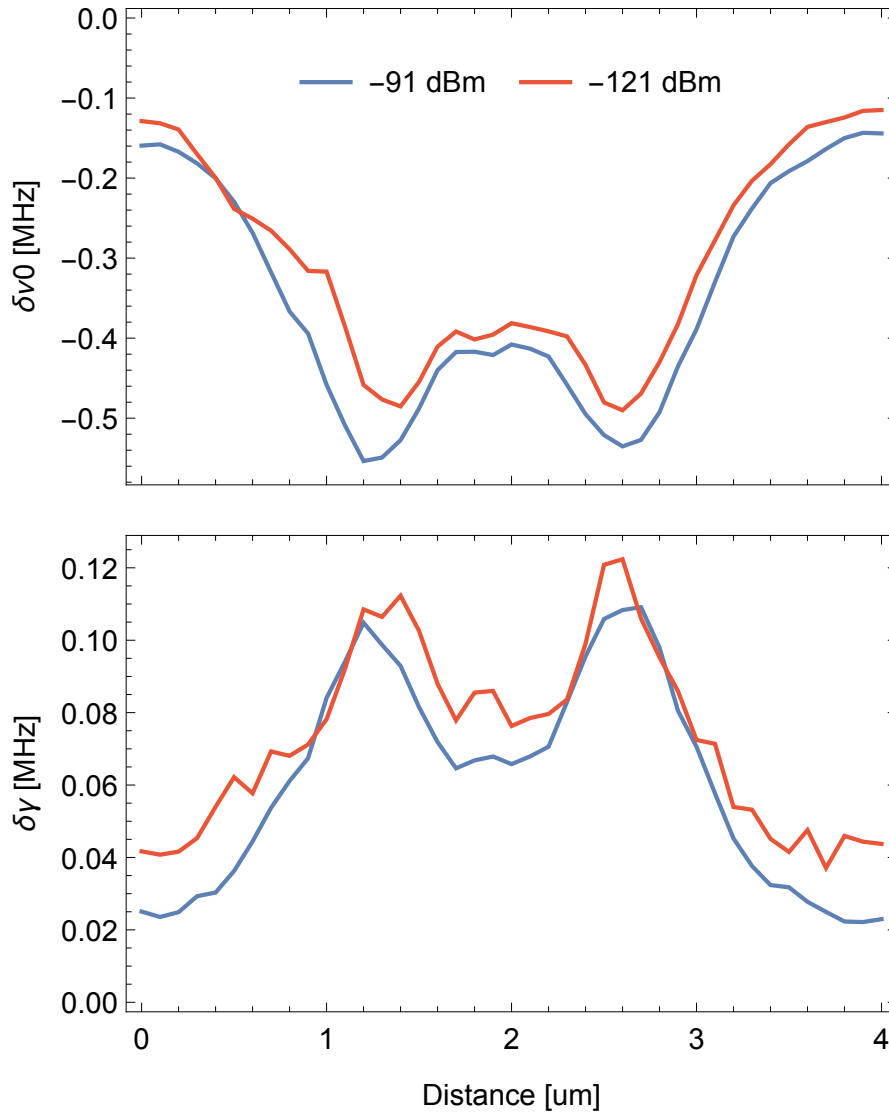
Figure 4.5: The estimates of δv_0 and $\delta \gamma$ depending on the position of the laser at the maximum and the minimum of the measured power. A peak current density at the edge is clearly visible.
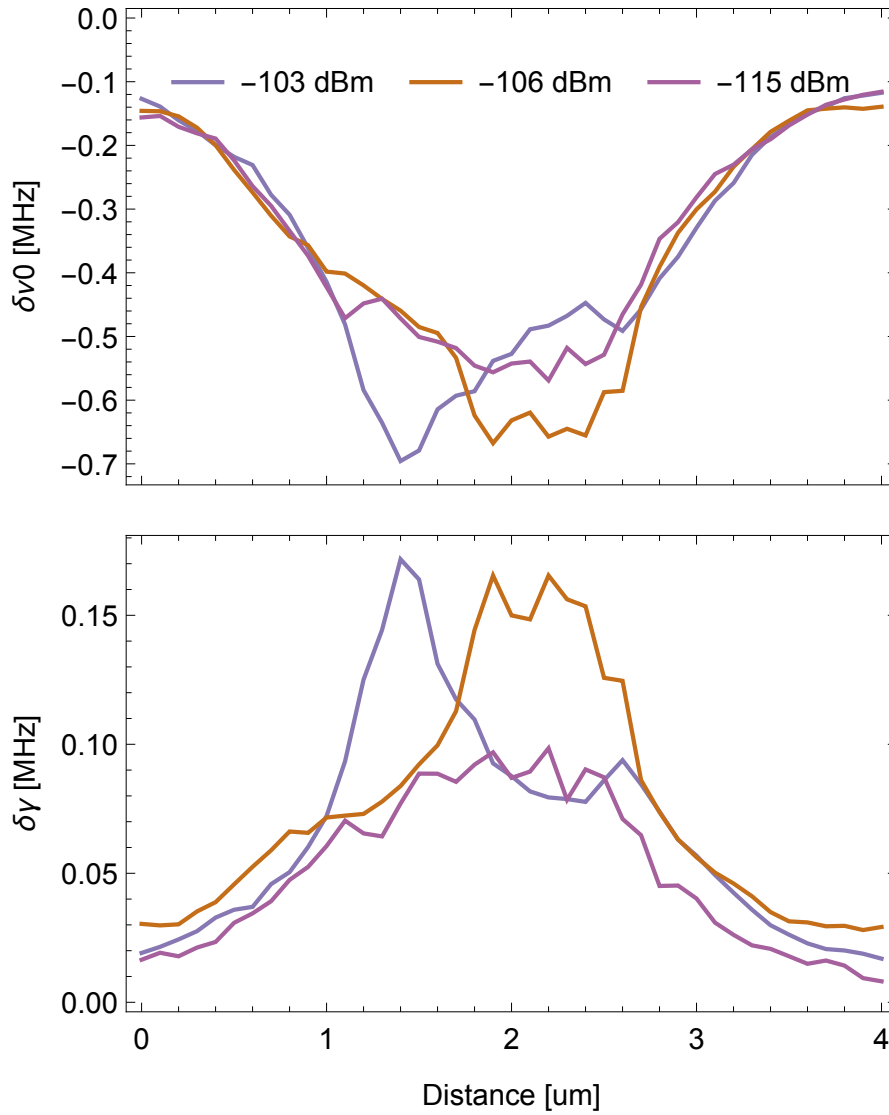
Figure 4.6: The estimates of δv_0 and $\delta \gamma$ for three measured powers show a different profile for the current density. This can be attributed to uncertainties in position and laser intensity.
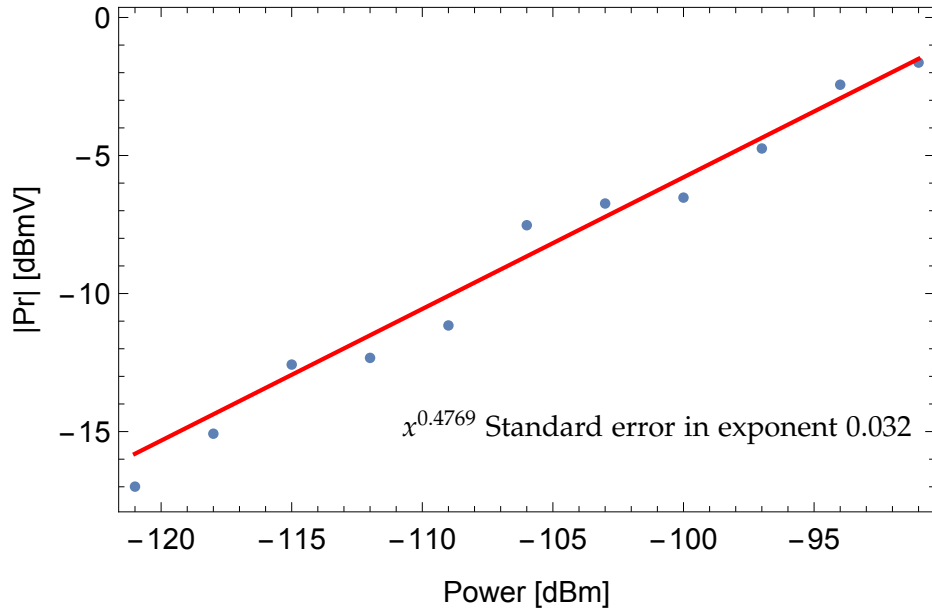
Figure 4.7: The photo response at the center of the inductor line with an exponential fit $x^{0.4769}$ for different RF powers.

4.3 Measuring the temperature dependence of the photo response

A change of temperature will lead to a change in the density of cooper pairs. This alone will shift and broaden the resonance without any laser shining on the metal. This dependence was measured and compared with theory by Chen [16].

The temperature dependence of the photo response, the shift in $\delta\nu_0$ and $\delta\gamma$, in respect to a modulated laser should show decreasing functions for both values on reducing the temperature [16].

In this experiment the lower temperature photo response, ranging from 3.05 K to 4.5 K at -97 dBm and 11.7 µW, was investigated. The static photo-response and the single point measurement were used to calculate $\delta\nu_0$ and $\delta\gamma$. This allows the comparison of the values gained through a fit and through the single point measurement.

The data from [16] shows an increase in $-\delta\nu_0$ and $\delta\gamma$ towards low temperatures. The increase can not be observed in this measurements. They show a monotonic decreasing function going to lower temperature for both parameters, as expected according to theory. The outliers are measurement errors due to the fluctuations of the laser power at the sample.

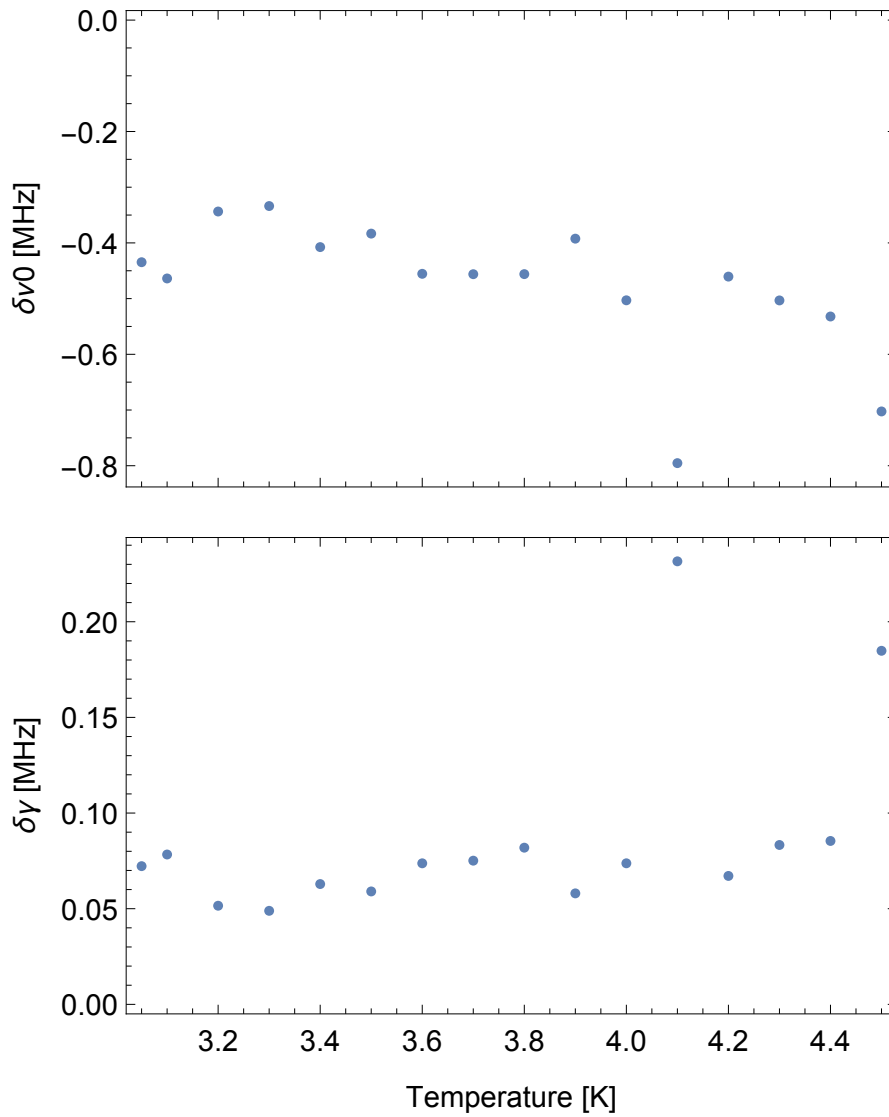Comparing the error between the two measurement methods, we see a rel-

Figure 4.8: The temperature dependence of $\delta\nu_0$ and $\delta\gamma$ at -97 dBm and 11.7 µW The two outliers are due to a changed laser intensity.
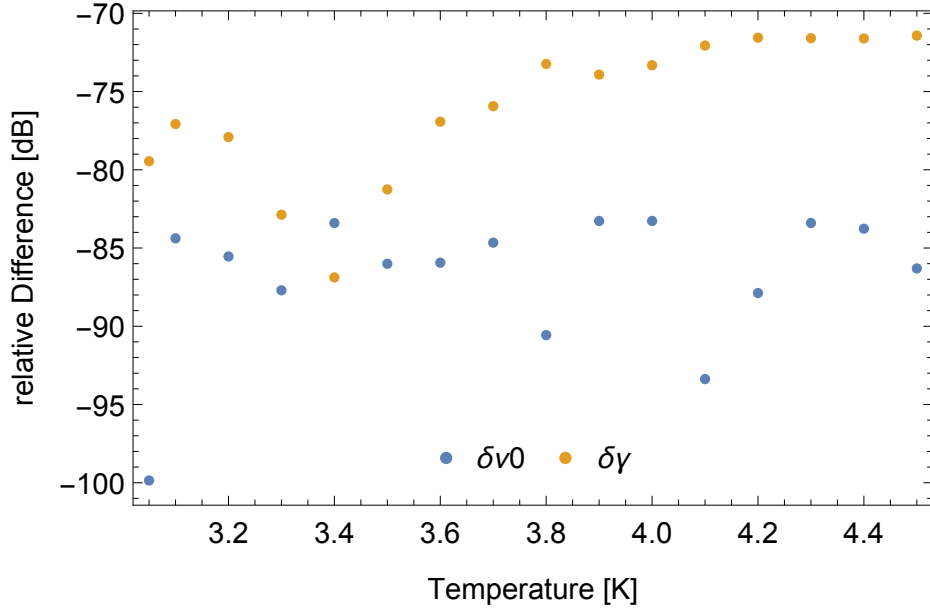
Figure 4.9: Comparing the relative difference between a fit to the static photo response measurement and the single point measurement method.

ative difference in the estimated values of less then -70 dB in fig. 4.9. This shows that the outliers are not only fitting errors, and demonstrates the usefulness of the single point measurement method again.

4.4 Time dependent photo response

The differential measurement scheme modulates the kinetic inductance at a frequency of 5 kHz. Higher frequency modulations would allow further investigations into the dynamics and new experiments. Recording a time-trace of the photo response allows to estimate the upper frequency limit of the internal dynamics as well as our setup.

The experiment was conducted at 3.3 K with -97 dBm RF power and a laser intensity of 11.7 µW. The AOM was connected to a signal generator without a stabilizing loop. Modulation frequencies of 5 kHz and 50 kHz were recorded using the FPGA with a 1 ns resolution. The signal was filtered using a moving-average filter with 8 bins.

Figure 4.10 shows the time measurement of the photo response. The rise time, corresponding to laser on to laser off, at 50 kHz from 10% to 90% is $T_{10\% \to 90\%} = 171$ ns and the fall time, corresponding to laser off to laser on, is $T_{90\% \to 10\%} = 104$ ns. This relaxation time leads to a lower bound for the
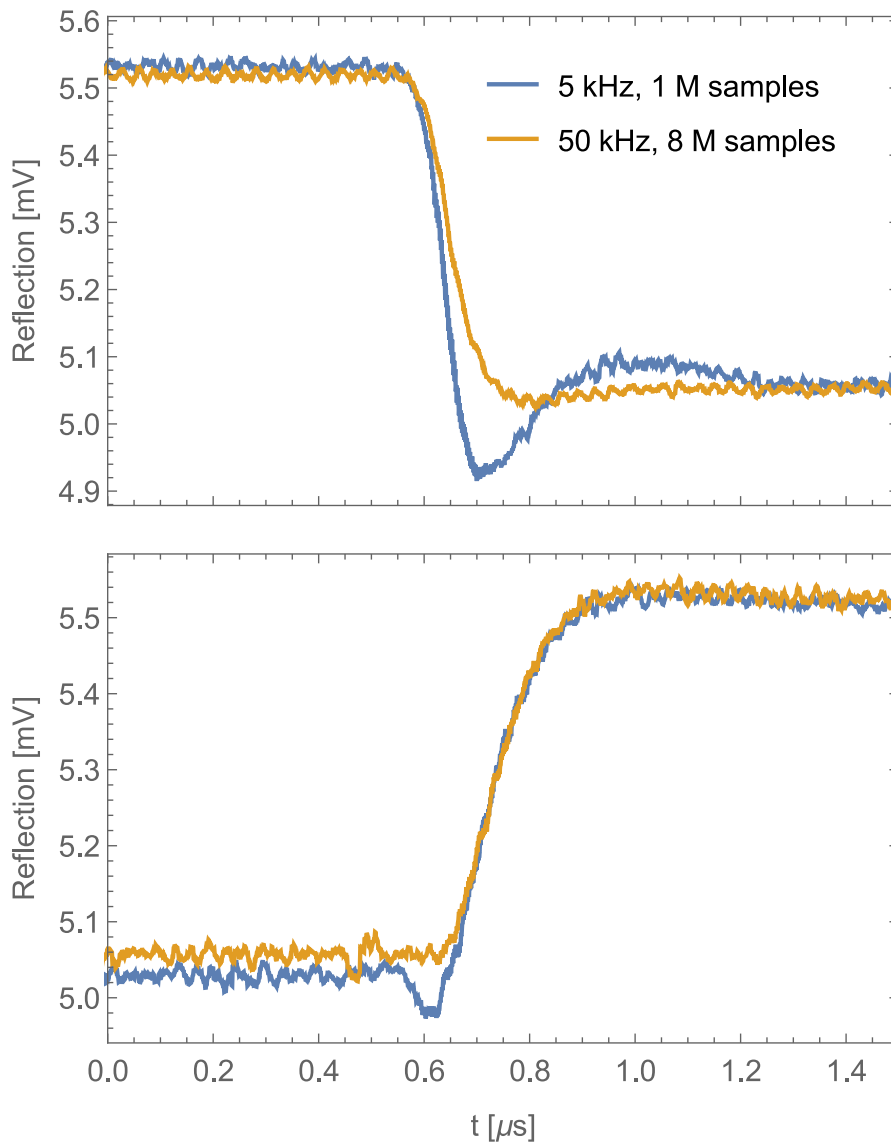
Figure 4.10: Time trace of laser off to laser on in the upper picture and laser on to laser off in the lower picture.

maximum frequency of the photo response of

$$\frac{1}{\max(T_{90\% \to 10\%}, T_{10\% \to 90\%})} = 5.84 \text{ MHz}. \tag{4.3}$$

The time constants in the experimental setup are given by the function generator with a rise time of 2.9 ns, the amplifier ZHL-03-5WF for the AOM with a range up to 300 MHz and the voltage controlled attenuator with up to 2500 MHz. The AOM offers a modulation frequency up to 8.8 MHz.

Measuring the rise of the intensity modulation of the laser was not possible due to the photo diode in the setup being limited to 2 MHz, limiting the resolution of the rise time to ≈ 200 ns [20].

Therefore it is not possible to rule out that the rise time is part of our laser modulation in the AOM. The difference between rise and fall time suggest an asymmetric process. Which there to our knowledge is no reason to suspect it in the AOM, the AOM amplifier or the voltage variable attenuator.

The lower limit for the relaxation rate can be calculated from the rise time assuming a first order decay by τ_{qp} of $\frac{T_{10\% \to 90\%}}{\log 9} = 77.4$ ns, where the division by logarithm of 9 is due to the 90% to 10% fall time.

Chen [16] estimates a recombination rate for this sample of $\tau_{qp} = 300$ ns, were the accuracy is limited through parameters and assumptions he made.

Chapter 5

Summary

This semester thesis investigates the photo response effect described in [16] and [8]. It proposes a new measurement scheme and compares it to the known ones. Additionally it investigates the temporal behavior of the photo response.

Chapter 1 introduces the reader to the topic. Chapter 2 explains the measurement setup and the newly build reference arm to allow a phase measurement. It also mentions the relocation of the setup into a new room and concludes with a verification of the working setup at the new location.

Chapter 3 explains in a brief summary the theory behind the photo response and the known measurement methods. It then introduces a new method that allows to measure the photo response for changed laser parameters with a single frequency measurement. This improves the measurement time dramatically and avoids fitting routines

Chapter 4 summarizes the results based on the measurements conducted:

   a. First the already known measurement methods introduced in section 3.3 were compared. After correcting for a difference due to the measurement method, the resulting relative error is less then -8 dB between the static measurement and the interleaved measurement method at the resonance of the system without laser. The newly proposed measurement method has a relative error compared to the static measurement that is smaller then -10dB at the resonance of the system without laser.

   b. The new measurement method was then used to investigate the spatial profile of the photo response at the center of the inductor of a lumped element harmonic oscillator. An increase of the photo response at the edge of the inductor was measured as already observed in the literature [9] in high temperature superconductors.

c. The time-dependent measurement conducted by [16] was repeated for temperatures between 3.05 K and 4 K. The increase of $\delta\nu_0$ and $\delta\gamma$, as measured by him, was not observed and the measurement followed the theory.

d. At last the temporal time evolution of the photo response was recorded an evaluated. The measurement show that the lower limit for the dynamics of the photo response is at 5 MHz. A different timescale in the Laser Off $\to$ Laser On and the Laser On $\leftarrow$ Laser Off change is observed were the first one is 60% faster. The reason is suspected to be in the dynamics of the photo response, but it has to be mentioned, that an asymmetric behavior in the laser modulation can not be ruled out due to measurement limitations. Estimating the recombination rate from the data leads to $\tau_{qp} = 77.4$ ns, compared to 300 ns estimated by Chen.

Due to this semester project the setup can be used at the new location with a more accurate measurement using the added reference arm. This allows to conduct fast spatial measurements with the new measurement method. For this the control of the positioning system should be implemented in CleanSweep. As a next step modulating the laser could allow to investigate the dynamics of the Cooper pairs. Classical Rabi-oscillations in two-level systems could be constructed by using the laser to create a tunable and time-dependent spring [21]. In circular structures the laser could be used to break the symmetry and split degenerate modes [22], or to construct the symmetry by correcting small errors due to manufacturing.

Appendix A

Information on the setup

A.1 Noisefloor of the setup

The noise floor of the setup was estimated by terminating the measurement chain at serveral points. The FIR filter was turned off, the power spectral density was calculated by using the correlator with the IQ signal on channel A and on channel B and there was 262144 measurements averaging. It was first terminated directly at the FPGA, after the down-conversion arm, after the FPGA, after a HEMT at 4 K in the fridge and at the input to the fridge. The measurement is plotted in fig. A.1.
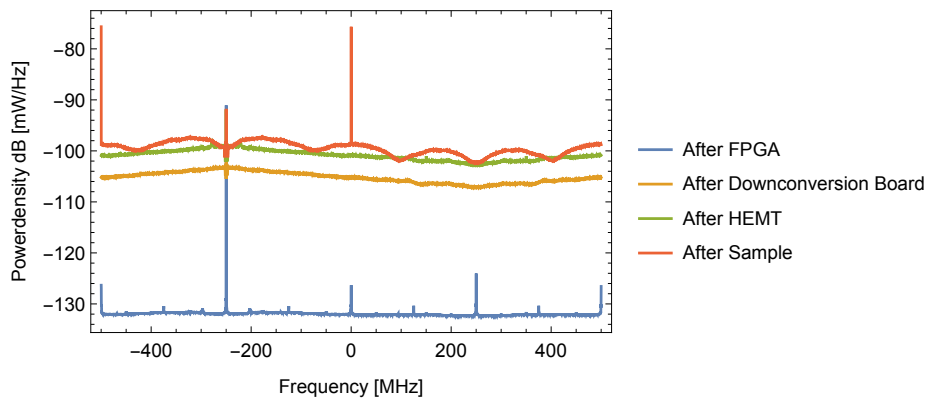

Figure A.1: Power density with the setup terminated at different stages in the experiment. Measured after a digital down-conversion from 250 MHz a clear DC peak can be seen at −250 MHz. The peaks at 0 Hz and −500 Hz in the measurement after the sample is our RF signal.

There is a difference of max. 2 dB between the noise level at the HEMT and after the sample, because of the high damping on the incoming line,

that removes thermal noise on the input. The noise from the HEMT gives an noise-increase of 5 dB. It has to be noted that the HEMT measured here, is the second HEMT in the setup, that is not connected to the sample, but terminated inside.

A.2 Cooldown of moved setup

The cooldown behavior of the sample at the old location and new location is compared in fig. A.2
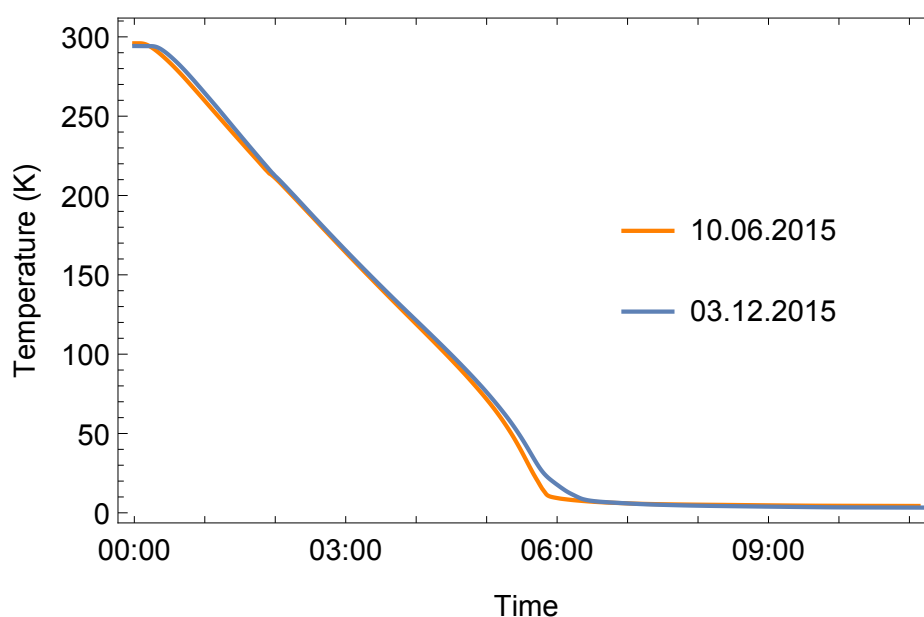

Figure A.2: Comparing two cooldown profiles from the old room and the new room. The temperature is measured at the sample holder.

A.3 Angle between laser and sample

The confocal microscope setup is tilted in respect to the mounted sample. This results in a change of the area seen, when changing the focus. Figure A.3 shows a sketch of the setup. ϕ is the angle between the normal of the axis of movement in $\hat{z}$ and θ is the angle between the microscope rig and the axis of movement. h_f is the height change in the focus and l_s is the shift in the field of view.

Looking at the edge of the inductor for $h_f = 3$ μm a shift in $\hat{y}$ direction of 4.2 μm and no shift in $\hat{x}$ direction was observed.

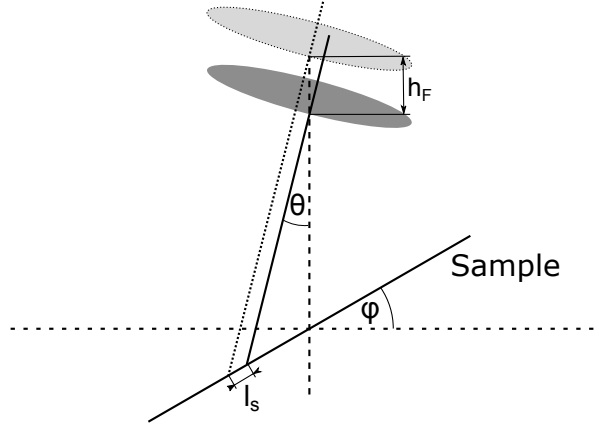*Figure A.3: The shift in field of view due to focus change.*

From fig. A.3 one can derive that

$$\frac{l_{\text{s}}}{h_{\text{f}}} = \frac{\sin\theta}{\cos(\theta + \phi)} \tag{A.1}$$

The angle of the sample was estimated by measuring the change of the height of the maximum focus, when moving in the $\hat{x}\hat{y}$-plane. The angle in $\hat{x}$ was 0.66 deg and in $\hat{y}$ it was 0.29 deg. The measured values for the change in focus are shown below.

direction	length	focus height-change
$\hat{x}$	200 μm	2.3 μm
$\hat{y}$	200 μm	1 μm

Combining this values using eq. (A.1) the angle θ of the laser is 54° in $\hat{y}$-direction and no measurable angle in $\hat{x}$-direction.

A.4   Sample layout

In this thesis the sample M36 LM1 1 was used. All the measurements were performed on port 9 of the sample containing a resonator with 27 inductor windings, 25 fingers at the capacitor and a 2 finger coupling capacitor. A picture of the resonator is given in fig. 3.2 and a mask layout is shown in fig. A.4.
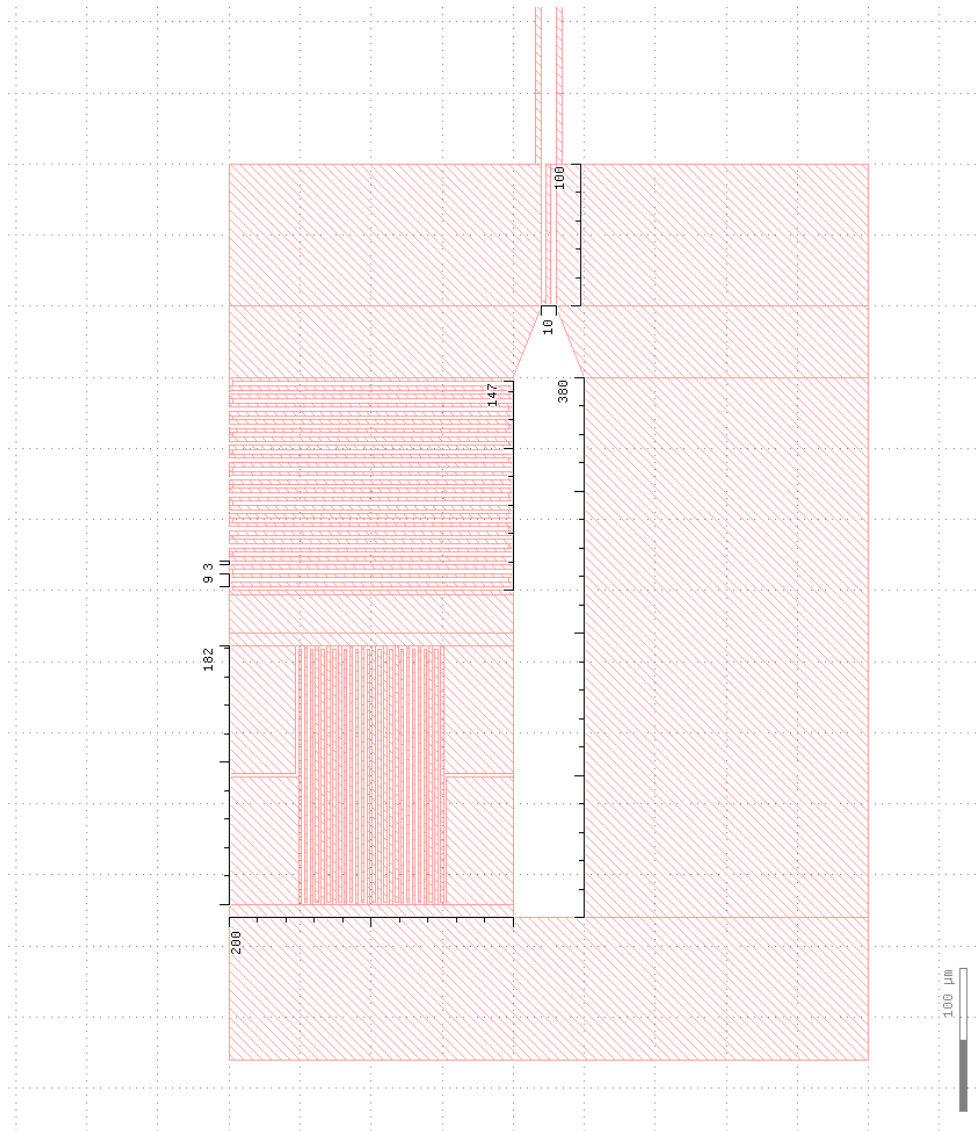
Figure A.4: The resonator used for all the experiments with 27 inductor windings and 25 fingers at the capacitor. The coupling is realized with a 2 finger capacitor.

A.5 Cabling of attoCube piezo stage

The attoCube system uses four types of connectors in our setup described in Table A.1.

Three stepper plugs and 3 piezo plugs are connected to the feed-through a plug as described in table A.2. The feed-through socket is then connected to the connector in the fridge as described in table A.3.
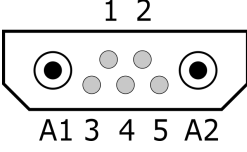
Table A.1: Connectors used in the system

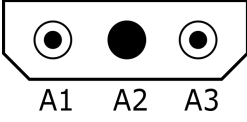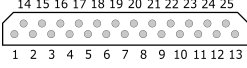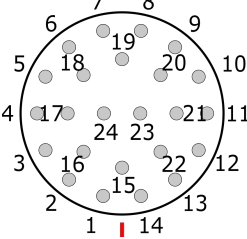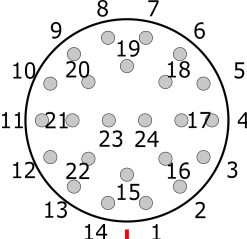|		
Stepper	A1 → -Out A2 → +Out	
Piezo	A1 → -Out A2 → +Out	1 → Sense- 2 → GND 3 → Sense+ 4 → RES-CON 5 → V0
Connector in fridge	Connected to feed-through socket	
Feed-through plug	Connected to ASC500 plugs	
Feed-through socket	Connected to connector in fridge.	

Table A.2: Connection between ASC500 and the feed-through plug

X-Scanner	A1 → 2	A2 → Shield	A3 →1		
Y-Scanner	A1 → 4	A2 → Shield	A3 →3		
Z-Scanner	A1 → 6	A2 → Shield	A3 →5		
X-Stepper	A1 → 8	A2 → 7	1,2,4 →11	3 → 10	5 → 9
Y-Stepper	A1 → 13	A2 → 12	1,2,4 →16	3 → 15	5 → 14
Z-Stepper	A1 → 18	A2 → 17	1,2,4 →21	3 → 20	5 → 19

Table A.3: Connection between feed trough socket and inside connector.

14 →18	13 →21	12 →9	11 →6
10 →19	09 →7	08 →22	07 →10
06 →23	05 →11	04 →24	03 →12
02 →25	01 →13	15 →5	22 →n.c.
21 →3	20 →16	19 →4	18 →20
17 →8	16 →17	24 →n.c.	23 →n.c.

35

A.6 Settings for the attoCube steppers

The settings in table A.4 were found through stepwise improvement of the recorded picture and the step performance. To optimize the values, one has to look at the position measurement in the time trace windows in ASC500 Changing the amplitude, and the frequency allows to find values so that only one step takes place every time the system goes to the next target position. This is not a big problem for the fast $\hat{x}$ axis, as it will be only one wrong measurement. For the slow $\hat{y}$ axis this will record a whole line at the wrong position.

If the steps are sometimes to far either the step size is too big or the frequency too high. Additionally the settling average allows to average out noise on the position measurement. The trade-off is between measurement time and accuracy.

The settling time can be found by looking at the position measurement and setting it higher then the time needed for the position measurement to be stable after one step.

Table A.4: Settings for the attoCube stepper measurement

	stepper direction	
	$\hat{x}$	$\hat{y}$
Amplitude	23 V	28.5 V
Frequency	500 Hz	750 Hz
Settling Time	4 ms	
Settling Average	10.24 ms	
Sample Time	5 ms	

Bibliography

[1] A. A. Houck, H. E. Tureci, and J. Koch, "On-chip quantum simulation with superconducting circuits," *Nat. Phys.*, vol. 8, pp. 292–299, Apr. 2012.

[2] R. Rouse, S. Han, and J. E. Lukens, "Observation of Resonant Tunneling between Macroscopically Distinct Quantum Levels," *Physical Review Letters*, vol. 75, pp. 1614–1617, Aug. 1995.

[3] J. M. Martinis and K. Osborne, "Superconducting Qubits and the Physics of Josephson Junctions," *arXiv:cond-mat/0402415*, Feb. 2004. arXiv: cond-mat/0402415.

[4] P. K. Day, H. G. LeDuc, B. A. Mazin, A. Vayonakis, and J. Zmuidzinas, "A broadband superconducting detector suitable for use in large arrays," *Nature*, vol. 425, pp. 817–821, Oct. 2003.

[5] Rösch, Markus, *Development of lumped element kinetic inductance detectors for mm-wave astronomy at the IRAM 30 m telescope.* PhD thesis, 2013.

[6] J. Federici, B. Greene, P. Saeta, D. Dykaar, F. Sharifi, and R. Dynes, "Cooper pair breaking in lead measured by pulsed terahertz spectroscopy," *IEEE Transactions on Applied Superconductivity*, vol. 3, pp. 1461–1464, Mar. 1993.

[7] A. P. Zhuravel, A. Sivakov, O. Turutanov, A. Omelyanchouk, S. Anlage, A. Lukashenko, A. Ustinov, and D. Abraimov, "Laser scanning microscopy of hts films and devices," *Low Temp. Phys.*, vol. 32, p. 6, 2006.

[8] H. S. Newman and J. Culbertson, "Measurement of the current density distribution in high temperature superconducting microstrip by means

of kinetic inductance photoresponse," *Microwave and Optical technology letters*, vol. 6, p. 13, 1993.

[9] J. C. Culbertson and H. Newman, "Optical probe of microwave current distributions in high temperature superconducting transmission lines," *J. Appl. Phys.*, vol. 84, p. 5, 1998.

[10] J. Chen and L. F. Wei, "Implementation speed of deterministic population passages compared to that of rabi pulses," *Phys. Rev. A*, vol. 91, p. 023405, Feb 2015.

[11] Attocube Systems AG, "Working principle - premium line positioners." `https://web.archive.org/web/20160217153555/http://www.attocube.com/attomotion/premium-line/introduction/#tab-2`, 2015. Accessed: 2016-02-17.

[12] Attocube Systems AG, "Datasheet - anpx101 steppers." `https://web.archive.org/web/20160217153219/http://marketing.attocube.com/acton/attachment/4434/f-013b/0/-/-/-/-/file.pdf`, 2015. Accessed: 2016-02-17.

[13] D. Bozyigit, "Correlation function measurements of a microwave frequency single photon source," Master's thesis, ETH Zurich, 04 2010.

[14] A. Rubio Abadal, "Josephson parametric amplifiers with lumped-element coupled resonators," Master's thesis, ETH Zürich, 2015.

[15] D. M. Pozar, *Microwave engineering*. John Wiley & Sons, Inc., 4th ed. ed., 2011.

[16] J. Chen, "Laser scanning microscopy of superconducting lumped element resonators," Master's thesis, ETH Zürich, 2015.

[17] M. Tinkham, *Introduction to Superconductivity*. McGraw-Hill International Editions, 1996.

[18] V. Novotny and P. P. M. Meincke, "Single superconducting energy gap in pure niobium," *Journal of Low Temperature Physics*, vol. 18, no. 1, pp. 147–157, 1975.

[19] R. E. Collin, *Foundations for microwave engineering*. IEEE Press series on electromagnetic wave theory, New York: IEEE Press, 2nd ed ed., 2001.

[20] E. Bogatin, "Rule of thumb #1: Bandwith of a signal from its rise time." `https://web.archive.org/web/20160217160305/http://www.edn.com/electronics-blogs/all-aboard-/4424573/`

Rule-of-Thumb--1--The-bandwidth-of-a-signal-from-its-rise-time, 2013. Accessed: 2016-02-17.

[21] M. Frimmer and L. Novotny, "The classical bloch equations," *arXiv:1410.0710*, 2014.

[22] Bargerbos, "Coupled lumped-element resonators with periodic boundary conditions," Master's thesis, ETHZ, 2015.

ETH

Eidgenössische Technische Hochschule Zürich
Swiss Federal Institute of Technology Zurich

Declaration of originality

The signed declaration of originality is a component of every semester paper, Bachelor's thesis, Master's thesis and any other degree paper undertaken during the course of studies, including the respective electronic versions.

Lecturers may also require a declaration of originality for other written papers compiled for their courses.

I hereby confirm that I am the sole author of the written work here enclosed and that I have compiled it in my own words. Parts excepted are corrections of form and content by the supervisor.

Title of work (in block letters):

Improved measurement method for spatial dependent photo response

Authored by (in block letters):

For papers written by groups the names of all authors are required.

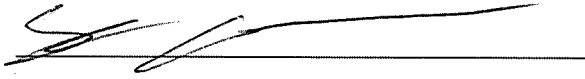| **Name(s):**	**First name(s):**
Gyger	Samuel

With my signature I confirm that
- – I have committed none of the forms of plagiarism described in the 'Citation etiquette' information sheet.
- – I have documented all methods, data and processes truthfully.
- – I have not manipulated any data.
- – I have mentioned all persons who were significant facilitators of the work.

I am aware that the work may be screened electronically for plagiarism.

Place, date

Zurich, 29.02.2016

Signature(s)

For papers written by groups the names of all authors are required. Their signatures collectively guarantee the entire content of the written paper.